Image formation in weak gravitational lensing by tidal charged black holes

Zsolt Horváth, László Rpád Gergely, David Hobill

Image formation in weak gravitational lensing by tidal charged black holes

Zsolt Horváth[1,2†], László Árpád Gergely[1,2‡], David Hobill[3*]

[1] Department of Theoretical Physics, University of Szeged, Tisza L krt 84-86, Szeged 6720, Hungary

[2] Department of Experimental Physics, University of Szeged, Dóm tér 9, Szeged 6720, Hungary

[3] Department of Physics and Astronomy, University of Calgary, Calgary Alberta T2N 1N4 Canada

[†]zshorvath@titan.physx.u-szeged.hu; [‡]gergely@physx.u-szeged.hu; [*]hobill@phas.ucalgary.ca

Abstract. We derive a generic weak lensing equation and apply it for the study of images produced by tidal charged brane black holes. We discuss the similarities and point out the differences with respect to the Schwarzschild black hole weak lensing, to both first and second order accuracy, when either the mass or the tidal charge dominates. In the case of mass dominated weak lensing, we analyze the position of the images, the magnification factors and the flux ratio, as compared to the Schwarzschild lensing. The most striking modification appears in the flux ratio. When the tidal charge represents the dominating lensing effect, the number and orientation of the images with respect to the optical axis resembles the lensing properties of a Schwarzschild geometry, where the sign associated with the mass is opposite to that for the tidal charge. Finally it is found that the brightness of images as a function of image separation in the case of tidal charged black holes obeys a power-law relation significantly different from that for Schwarzschild black holes. This might provide a means for determining the underlying spacetime structure.

1. Introduction

Gravitational lensing has become a useful tool in measuring certain properties of gravitational fields ever since the beginnings of general relativity. While the initial observations of gravitational lensing were used to verify the theoretical predictions of general relativity, it has now been employed to study the large scale structure of the Universe, to determine behaviour of compact stellar objects and to search for dark matter candidates. In what follows we propose the idea that gravitational lensing might also be used to determine which among various gravitational theories is correct. It is already well known that the predictions of bending angles computed from Newtonian gravity compared to those obtained from Einstein's gravity differ by a factor of two. Therefore using gravitational lensing a means for exploring the differences between competing gravitational theories may well provide a technique that can be employed to determine the dimensionality of spacetime, or the coupling of matter and fields to the gravitational field or even to distinguishing among different formulations of gravity theories.

In general the path taken by photons in a gravitational field provide a number of different effects that can be measured using current state of the art telescopes. The first and most obvious one is the production of multiple images and the relative separation of those images. Secondly gravitational lensing can produce a change in brightness of the images depending on how much bending a group of initially parallel rays undergoes. Finally if the source or lensing object has a time dependency, the changes in arrival times of light signals can provide a very accurate measurement of some spacetime properties.

In this paper, we discuss the formation of images (i.e. their location and brightness) for some black holes that are predicted to exist in 5-dimensional brane-world theories. By computing the bending angles and image brightness changes that can occur due to the passage of photons past the objects described by black hole solutions of the theory, we should be able to determine enough of the properties of the lensing object to distinguish a general relativistic black hole from that predicted by an alternative theory.

Brane-world models have standard-model matter confined to a 3+1 dimensional hypersurface, and gravity acting in a higher-dimensional non-compact space-time. Such models have attracted much attention in recent years, both as candidate theories meant to solve the hierarchy problem and predicting modified cosmological evolution [1]. Higher codimension branes were considered in connection with conical singularities [2], [3]. For a codimension-one brane-world, matter is generated on the brane by the junction conditions though the brane representing a discontinuity in the extrinsic curvature [4]-[7]. Although the early expectation to replace dark energy was not met, codimension-one brane-worlds still can produce alternative explanations for dark matter [8]-[10]. Therefore the study of localized matter configurations, in particular black hole solutions admitted in brane-world theories became important.

Analytic black hole solutions include six-dimensional locally Schwarzschild solutions [11]; static five-dimensional black holes localized on the brane, with the horizon decaying

in the extra dimension and generated by energy condition violating shells [12], [13]; and black holes with a radiating component in the extra dimension [14]. Numerically small brane black holes (compared to the five-dimensional curvature) were shown to exist as five-dimensional Schwarzschild solutions [15] in asymptotically five-dimensional Anti de Sitter space-time.

The four-dimensional Schwarzschild metric can be also extended into the fifth dimension as a black string [16], which due to the Gregory-Laflamme instability [17] can pinch off, leading to a black cigar metric [18] (although under very mild assumptions, classical event horizons will not pinch off [19]). Gravity wave perturbations of such a black-string brane-world were computed in Ref. [20].

The perturbative analysis of the gravitational field of a spherically symmetric source in the weak field limit in the original Randall-Sundrum setup (Schwarzschild black hole on a brane embedded in Anti de Sitter five-dimensional space-time) has shown corrections to the Schwarzschild potential scaling as r^{-3} [21], [22] and [23]. However if the Schwarzschild black hole is embedded in another higher-dimensional space-time, this scaling would not apply [24]. Both weak [25], [26] and strong [27] gravitational lensing of various brane black holes were discussed, the topic being reviewed in Ref. [28].

The effective Einstein equation on the codimension-one brane admits a spherically symmetric vacuum solution characterized by two parameters: the mass m and a tidal charge q, the latter arising from the Weyl curvature of the 5-dimensional space-time in which the brane is embedded [29]:

$$\begin{aligned} ds^2 = & -f(r)\,dt^2 + f^{-1}(r)\,dr^2 + r^2\left(d\theta^2 + \sin^2\theta d\varphi^2\right) , \\ f \ = & 1 - \frac{2m}{r} + \frac{q}{r^2} . \end{aligned} \tag{1}$$

For $q \leq m^2$ this represents a black hole with horizons given by $r_\pm = m \pm (m^2 - q)^{1/2}$. For $q < 0$ only r_+ is positive, therefore there is only one horizon. For $q = 0$ the line element describes the Schwarzschild metric and for $0 < q \leq m^2$ it is formally identical to the general relativistic Reissner-Nordström electro-vacuum solution with electric charge $Q = q^{1/2}$. In the limit $q = m^2$ the metric becomes extremal, such that the two horizons coincide. For $q > m^2$ there is no horizon at all. The metric is singular at $r = 0$, thus it describes a naked singularity. It should be noted that a negative tidal charge strengthens gravity (the horizon is outside the Schwarzschild radius $2m$), such that $q < 0$ contributes to the localization of gravity on the brane. A positive tidal charge weakens gravity, both horizons lying below the Schwarzschild radius for $0 < q \leq m^2$, and obstructing the apparition of a horizon at all for $q > m^2$.

Observations on light deflection could in principle constrain both the lensing black hole parameters and the underlying gravitational theory. The lensing properties of a Schwarzschild geometry were thoroughly investigated in Refs. [30], [31]. Recently in Ref. [32] the deflection angle of light rays passing near the tidal-charged brane black hole was computed up to the second order in the perturbation theory. The Hamiltonian method gave identical results to the previously employed Lagrangian method [33]. The

light deflection was derived in terms of the small parameters $\varepsilon := m/b$ and $\eta := q/b^2$. Here b is the impact parameter, defined as the distance of the lensing object to the straight line trajectory, which would occur in the absence of the lensing object. The deflection angle to second order accuracy is

$$\delta = 4\varepsilon - \frac{3}{4}\pi\eta + \frac{15}{4}\pi\varepsilon^2 - 16\varepsilon\eta + \frac{105}{64}\pi\eta^2 \ . \tag{2}$$

A first confrontation with Solar System measurements in Refs. [32], [34] led to constraints on q and on the brane tension λ.

Further exploring the consequences of the result (2), in the present paper we study the formation of images and their magnification factors in the tidal charged black hole geometry, focusing on the similarities and differences with the purely general relativistic case.

In the case of weak lensing where the latter black hole solutions differ from standard general relativistic black holes, we are able to develop a perturbative computation of the bending angles and image brightnesses that can be expected when the black hole masses produce the dominant effect. However the restriction to objects with weak tidal charge (compared to mass) is not necessary. As long as the impact parameter or distance of closest approach for the light ray remains large compared to a natural length scale associated with the tidal charge, the weak field limit is maintained and tidally charged black hole light bending effects can also be computed.

In Section 2 we study the weak lensing under quite generic circumstances. We derive a lens equation for weak lensing, which will allow for a study of the lensing and image formation to second order accuracy in the chosen small parameters. This lens equation is more generic than, and reduces to, the Virbhadra-Ellis equation [31]-[35] in a properly defined approximation. We give the explicit form of both lens equations applied to the tidal charged black hole in the Appendix, in order to see at which order the differences arise.

In Section 3 we employ the deflection angle (2) in our lens equation and obtain an approximate equation for weak lensing of the tidal charged black hole in a form of a cubic polynomial. For later comparison we also review here the lensing by Schwarzschild black holes, which arises in our formalism to first order when the mass parameter dominates over the tidal charge parameter.

In Section 4 we discuss the corrections in the location of the images and magnification factors, by including the contributions quadratic in the mass parameter and linear in the tidal charge parameter. This analysis leads to results that are similar to the general relativistic Reissner-Nordström black hole lensing, some of them discussed in Ref. [36]. Despite q being similar to the square of the electric charge of the Reissner-Nordström black hole, the case of a negative tidal charge is without counterpart in general relativity.

Section 5 contains the analysis of the case, where the tidal charge dominates over the mass, by keeping only the first order tidal charge contribution. We determine the image locations and the magnification factors. In Section 6 we discuss the second order

corrections to the above case, by including contributions linear in the mass and quadratic in the tidal charge.

We summarize our findings in the Concluding Remarks. Our choice of units is given by $G = 1 = c$.

2. The lens equation

In the lensing geometry the line connecting the lensing object (L) and the observer (O) defines the optical axis. Relative to this axis the source location (S) makes an angle $\beta = \widehat{LOS}$ from the optical axis, chosen positive by convention (such that S is always located "above" the optical axis, see Fig 1). Due to the lensing effect however the source appears shifted away, and this is called the image (I). The angle $\theta = \widehat{IOL}$ indicates the image position and it can be either positive (for images above the optical axis) or negative (for images below the optical axis). Let us denote $s =$sgn θ, such that $|\theta| = s\theta$. Finally, the deflection angle $\delta = \widehat{SAI}$ characterizes the change in the direction of light due to the lensing object. We follow the convention that $\delta > 0$ whenever the light is bent towards the optical axis and $\delta < 0$ otherwise, cf. Ref [31]. Projecting the points S and I onto the optical axis ($\overline{OL}$) defines the distances $|\overline{LN}|$ or D_{ls} from the lensing object and $|\overline{ON}|$ or D_s from the observer. The observer-lensing object distance is $D_l = D_s - D_{ls}$.

From Fig 1 the angle $\widehat{ASI} = \pi/2 + |\theta| - \delta$. Then the sine theorem applied in the triangle ASI reads

$$\frac{\overline{NI} - s\overline{NS}}{\sin\delta} = \frac{\overline{OI} - \overline{OA}}{\cos\left(\delta - |\theta|\right)} \ . \tag{3}$$

(We have taken into account the particularities of the configurations indicated on Fig 1 by including the sign s, whenever necessary.) By multiplying the equation (3) with $\sin\delta\cos\left(\delta - |\theta|\right)/\overline{OI}$ we obtain

$$\left(\frac{\overline{NI}}{\overline{OI}} - s\frac{\overline{NS}}{\overline{OI}}\right)\cos\left(\delta - |\theta|\right) = \left(1 - \frac{\overline{OA}}{\overline{OI}}\right)\sin\delta \ . \tag{4}$$

We rewrite the left hand side by expressing $\sin|\theta|$, $\cos\theta$ and $\tan\beta$ from the triangles ONI and ONS. In the second term on the right hand side we rewrite $\overline{OI} = D_s\cos\theta$. We note that the point A where the trajectory is bent is defined such that $\widehat{OAL} = \widehat{SAL} = (\pi - \delta)/2$. Then $\widehat{OLA} = \pi/2 + |\theta| + \delta/2$, and the sine theorem for the triangle LAO gives

$$\frac{\overline{OA}}{\cos\left(\frac{\delta}{2} - |\theta|\right)} = \frac{D_l}{\cos\frac{\delta}{2}} \ , \tag{5}$$

such that Eq. (4) becomes

$$\begin{aligned} 0 = {} & \frac{2D_l}{D_s}\cos\left(\frac{\delta}{2} - |\theta|\right)\cos|\theta|\sin\frac{\delta}{2} \\ & + \cos\left(\delta - |\theta|\right)\left(\sin|\theta| - s\cos|\theta|\tan\beta\right) - \sin\delta \ . \end{aligned} \tag{6}$$

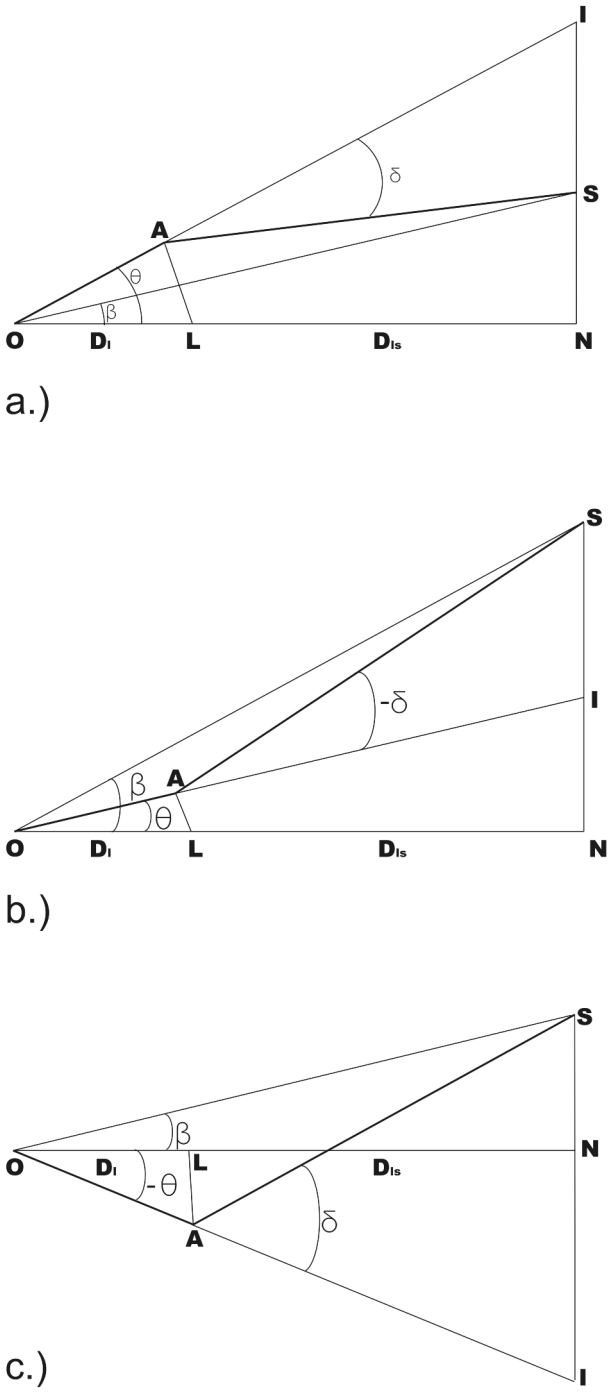

Figure 1. Schematic representation of typical lensing configurations. The light emitted from the source S, is deflected by the lensing object L such that the observer at O will see the image I. The angles β and θ represent the angles spanned by the real and apparent directions of the source with the line connecting the observer and the lensing object. The light is bent towards the optical axis, while it passes above (a) or below (c) the lensing object. Case (b) refers to a repulsive interaction, which will also be encountered in this paper as a limiting sub-case. On the figures we represent the (positive) length of the arcs, expressed as β, $|\theta| = s\theta$, $+\delta$ for (a), (c) and $-\delta$ for (b).

We would like to stress that this is an *exact lens equation* in the weak lensing approximation, as it was obtained exclusively by trigonometric considerations, and no power series expansions of trigonometric functions were applied.‡ We will employ Eq. (6) to derive the approximate lensing equation to the accuracy required by our approach.

Before doing so, we comment that in the particular configuration of O, L and S being aligned (such that $\beta = 0$) the above equation reduces to

$$0 = D_l \sin|\theta| + D_{ls} \sin(|\theta| - \delta) \ , \tag{7}$$

the solution of which gives the angle for the formation of the Einstein ring:

$$|\theta| = \arctan \frac{D_{ls} \sin\delta}{D_l + D_{ls}\cos\delta} \ . \tag{8}$$

The usefulness of this expression is however limited, as δ is not an observable quantity.

Secondly, we discuss the limit in which an approximate lens equation, one that is frequently employed in the literature, arises. For this, we need to assume $\overline{LA} \perp \overline{ON}$ (see Fig. 1 of Ref. [30]), which introduces an error of order of the angle of deviation from perpendicularity, which is $\theta - \delta/2$. Then to first order in $\epsilon := \delta - 2|\theta|$ the lens equation (6) becomes

$$\begin{aligned} 0 = \ & \tan|\theta| - s\tan\beta - \frac{D_{ls}}{D_s}\tan|\theta| - \frac{D_{ls}}{D_s}\tan(\delta - |\theta|) \\ & + \epsilon\tan|\theta|\left(s\tan\beta + \frac{D_{ls}}{D_s}\tan|\theta|\right) + \mathcal{O}\left(\epsilon^2\right) \ . \end{aligned} \tag{9}$$

The expansion in ϵ of the term $\tan(\delta - |\theta|)$ contains the linear contribution $\epsilon/\cos^2|\theta|$. To linear order in ϵ, the last term can be approximated by replacing β with its zeroth order expression: $s\tan\beta = \tan|\theta| - 2(D_{ls}/D_s)\tan|\theta|$, obtaining $\epsilon(D_l/D_s)\tan^2|\theta|$. For small $|\theta|$, this last contribution can be safely dropped as compared to $\epsilon/\cos^2|\theta|$. The terms to keep are

$$0 = \tan|\theta| - \tan(s\beta) - \frac{D_{ls}}{D_s}\left[\tan|\theta| + \tan(\delta - |\theta|)\right] \ . \tag{10}$$

With a change in notation where $|\theta| \to \theta_{VE}$, $s\beta \to \beta_{VE}$ which corresponds to the change in the convention of which angles are defined to be positive (specifically $\beta \geq 0$ in our approach and $\theta_{VE} \geq 0$ in Refs. [31]-[35]), the equation (10) is known as the Virbhadra-Ellis lens equation. From the way it arises in our formalism, we can tell that this equation is valid for small angles $|\theta|$ and to first order accuracy in $\delta - 2|\theta|$. This quantity vanishes if S, L and O are collinear ($\beta = 0$) and L is midway between S and O. It is therefore expected, that the predictions of the more exact lens equation (6) will differ from the predictions of Eq. (10) in asymmetric setups of S and O with respect to L.

Since we are interested in possibly higher order contributions, characterizing the lensing by tidal charged brane black holes and naked singularities with tidal charge, we need to improve the level of approximation employed in Eq. (10). Therefore we start our

‡ A more general lens equation is also known for generic curved space-times [37].

investigations on the brane-world lensing process from the lens equation derived here, Eq. (6) and we will employ a higher order expansion than the one leading to Eq. (10). We have also adopted the convention $\beta > 0$ as this will turn useful in the discussion of the second-order effects.

The lens equation (6) presented here is obtained solely from the geometry of the paths taken by both the deflected and undeflected light rays. It relates the angles θ, β and δ to each other through the relations among the trigonometric functions of those angles. The lens equation in this form does not care whether the lensing carried out by an optical instrument or a gravitational lens.

When the bending is due to gravitational effects, the deflection angle δ (characterizing the strength of the bending) can be derived from the null geodesic equations. For weak lensing, the deflection angle can be computed using a set of expansion parameters that characterize the geometry of the black hole spacetime. In the cases studied in this paper we use the mass and tidal charge divided by a characteristic length scale. The lens equation can then be applied along with an expression for the bending angle δ to obtain the image locations θ given a source position β.

The issue that arises is to ensure that the accuracy of the lens equation matches the level of accuracy of the approximation in the deflection angle. If the lens equation is accurate only to linear order in the angles and the deflection angle is good to third order in the expansion parameters, then there is a loss of accuracy in the former that no longer makes it suitable for higher order computations. If this is not properly taken into account, errors will arise. On the other hand two different expressions for the lens equations can lead to indistinguishable results if they agree to within the same order of approximation.

3. Second order lens equation in the mass and tidal charge

In order to find the position of the images, first the expansion (2) of the deflection angle δ should be inserted in the lens equation (6), secondly the approximations following from the weak lensing approach are carried out. An inconvenience in proceeding this way is that the impact parameter $b = D_l \sin|\theta|$ entering in the definitions of the small parameters ε and η depends on θ. Therefore we introduce the alternative set of small parameters

$$\bar{\varepsilon} = \frac{m}{L} \ , \quad \bar{\eta} = \frac{q}{L^2} \ , \tag{11}$$

with $L = D_s D_l / D_{ls}$. A series expansion of Eq. (6) accurate to second order in both small parameters gives

$$0 = L_0 + \bar{\varepsilon} L_{10} + \bar{\eta} L_{01} + \bar{\varepsilon}^2 L_{20} + \bar{\varepsilon}\bar{\eta} L_{11} + \bar{\eta}^2 L_{02} \ . \tag{12}$$

Here

$$\begin{aligned} L_0 &= \cos^2\theta \ (\tan|\theta| - s\tan\beta) \ , \\ L_{10} &= -4\cos|\theta| \left(s\frac{L}{D_l}\tan\beta + \cot|\theta| \right) \ , \end{aligned}$$

$$
\begin{aligned}
L_{01} &= \frac{3\pi}{4}\frac{L}{D_l}\cot|\theta|\left(s\frac{L}{D_l}\tan\beta+\cot|\theta|\right)\ ,\\
L_{20} &= \frac{L}{4D_l}\cot|\theta|\left[s\frac{L}{D_l}\tan\beta\left(32\cot|\theta|-15\pi\right)-32-15\pi\cot|\theta|\right]\ ,\\
L_{11} &= -\frac{L^2}{D_l^2}\frac{\cos|\theta|}{\sin^2|\theta|}\left[s\frac{L}{D_l}\tan\beta\left(3\pi\cot|\theta|-16\right)-3\pi-16\cot|\theta|\right]\ ,\\
L_{02} &= \frac{3\pi}{64}\frac{L^3}{D_l^3}\frac{\cos|\theta|}{\sin^3|\theta|}\left[s\frac{L}{D_l}\tan\beta\left(6\pi\cot|\theta|-35\right)-6\pi-35\cot|\theta|\right]\ . \qquad (13)
\end{aligned}
$$

The zeroth order contribution L_0 shows that without the black hole ($m = 0 = q$) there is no deflection, $\theta = \beta$.

Without the tidal charge and to first order in $\bar{\varepsilon}$ we obtain the standard Schwarzschild lensing as

$$
0 = \cos|\theta|\left[\cos|\theta|\ \ (\tan|\theta|-s\tan\beta)-4\bar{\varepsilon}\left(\cot|\theta|+s\frac{L}{D_l}\tan\beta\right)\right]\ . \qquad (14)
$$

From the lensing geometry (see Fig 1, with the remark that the involved distances are large and the deflection is relevant only for the trajectories crossing nearby the lensing object) we can safely conclude, that $\beta = \mathcal{O}(\theta)$. Assuming that $\bar{\varepsilon} = \mathcal{O}(\theta^2)$ (we will see that in our approach this condition is necessary for weak lensing), to leading order we obtain

$$
0 = \ \theta^2-\beta\theta-4\bar{\varepsilon} \equiv \mathcal{S}\ , \qquad (15)
$$

with the known solutions

$$
\theta_{1,2} = \frac{\beta\pm\sqrt{\beta^2+16\bar{\varepsilon}}}{2}\ . \qquad (16)
$$

The position of the images is represented on Fig 2. With perfect alignment of the source, lensing object and observer along the optical axis we get the angular radius of the Einstein ring $\theta_E = 2\bar{\varepsilon}^{1/2}$. This verifies the correctness of our assumption on the order of $\bar{\varepsilon}$.

For a hypothetical negative lensing mass there are still two images [38], provided the discriminant stays non-negative, thus for $\beta^2 - 16|\bar{\varepsilon}| \geq 0$. This time however both images have a positive θ. At equality the two images coincide.

For a lens with axial symmetry the magnification factor (the ratio of the solid angle subtended by the image divided by the solid angle subtended by the source) is given by [39], [40]

$$
\mu = \left|\frac{\theta}{\beta}\frac{d\theta}{d\beta}\right|\ , \qquad (17)
$$

where both θ and β are small angles. For a Schwarzschild lens, we substitute the images (16) and obtain

$$
\mu_{1,2} = \frac{1}{4}\left(\frac{1}{\beta}\sqrt{\beta^2+4\theta_E^2}+\frac{\beta}{\sqrt{\beta^2+4\theta_E^2}}\pm 2\right)\ . \qquad (18)
$$

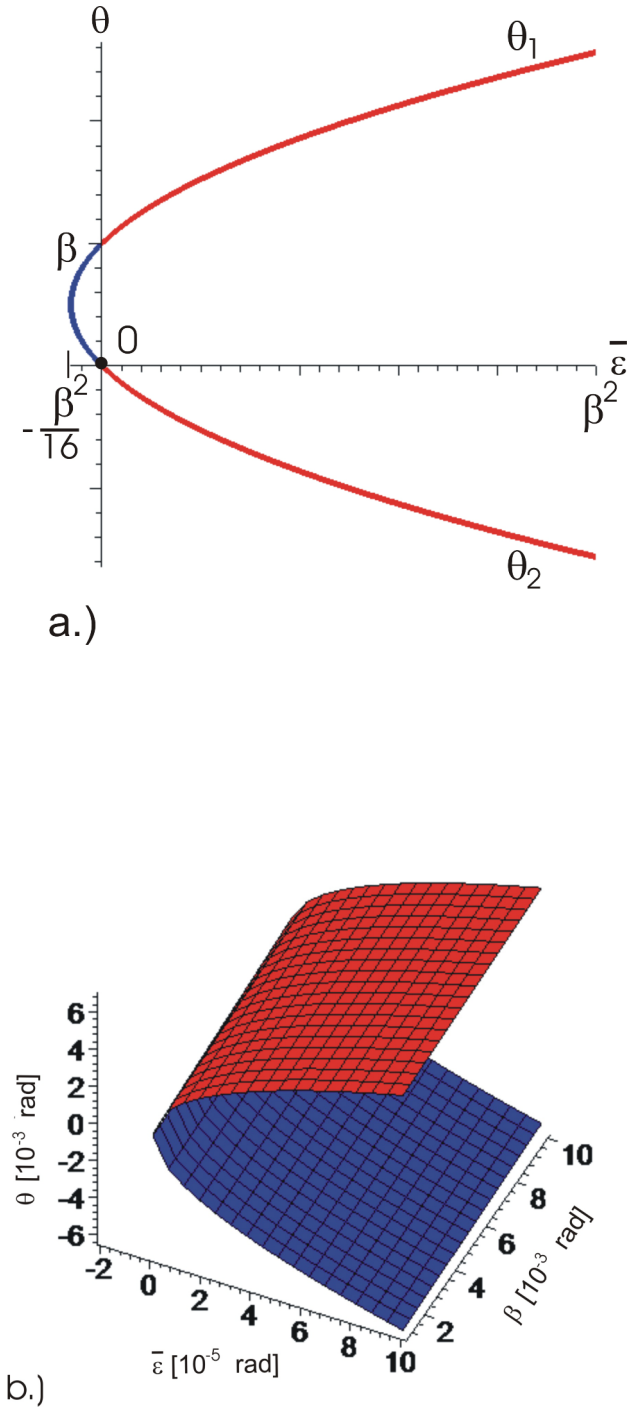

Figure 2. (Colour online.) When the mass dominates over the tidal charge in the lensing, the images arise as in the Schwarzschild case. (a) The position θ (in units β) of the images for Schwarzschild black holes is characterized by the parameter $\bar{\varepsilon}$ (in units β^2), $\beta > 0$ indicating the real position of the source. For positive mass ($\bar{\varepsilon} > 0$) there are two images, situated above and below the optical axis. For negative mass ($\bar{\varepsilon} < 0$) both images lie above the optical axis. The images coincide for $\bar{\varepsilon} = -\beta^2/16$. For each β, the negative masses with $\bar{\varepsilon} < -\beta^2/16$ do not allow for any image. (b) θ as function of $\bar{\varepsilon}$ and β. With decreasing β, the images shrink accordingly. At $\beta = 0$, the angle θ represents the angular radius of the Einstein ring (therefore the $\beta = 0$ section of the surface is symmetric with respect to $\theta = 0$).

When $\beta \to 0$

$$\begin{aligned}
\mu_{1,2} &= \frac{\theta_E}{2\beta} \pm \frac{1}{2} + \frac{3\beta}{8\theta_E} + \mathcal{O}\left(\beta^2\right) \ , \\
\frac{\mu_1}{\mu_2} &= 1 + \frac{2\beta}{\theta_E} + \frac{2\beta^2}{\theta_E^2} + \mathcal{O}\left(\beta^3\right) \ , \\
\theta_{1,2} &= \pm\,\theta_E + \frac{\beta}{2} \pm \frac{\beta^2}{8\theta_E} + \mathcal{O}\left(\beta^3\right) \ ,
\end{aligned} \tag{19}$$

thus the magnification factors diverge, while their ratio (the flux ratio) μ_1/μ_2 goes to unity. So far we have reproduced known results.

In what follows, we will discuss two novel applications:

A) The case when the tidal charge contributes to second order, thus $\mathcal{O}(\bar{\eta}) < \mathcal{O}(\bar{\varepsilon})$. This case will be discussed to second order accuracy. (For positive tidal charge, with the replacement $q \to Q^2$ we recover Reissner-Nordström lensing.)

B) The case when the tidal charge dominates, thus $\mathcal{O}(\bar{\varepsilon}) < \mathcal{O}(\bar{\eta})$. Here for simplicity first we go only to first order in $\bar{\eta}$, this being formally equivalent to dropping all $\bar{\varepsilon}$ terms. Subsequently, we will analyze the second order corrections.

In what follows, the black hole parameters will be related to $\mathcal{O}(\theta)$ by assumptions well justified case-by-case. Equivalently, we will investigate the weak lensing properties of tidal charged black holes in the corresponding ranges of its parameters.

4. Mass dominated weak lensing to second order

Under the assumptions A) of Section 3 the terms $\bar{\varepsilon}\bar{\eta}$ and $\bar{\eta}^2$ can be dropped from the lens equation (12). By taking as before $\bar{\varepsilon} = \mathcal{O}(\theta^2)$, then $\bar{\eta} \leq \mathcal{O}(\bar{\varepsilon}^2) = \mathcal{O}(\theta^4)$ and keeping only the first and second order terms we obtain

$$0 = \frac{\mathcal{S}}{\theta} + s\gamma \frac{\bar{\eta} - 5\bar{\varepsilon}^2}{\theta^2} \ , \tag{20}$$

or

$$0 = \theta^3 - \beta\theta^2 - 4\bar{\varepsilon}\theta + s\gamma\left(\bar{\eta} - 5\bar{\varepsilon}^2\right) \ . \tag{21}$$

where we have introduced the notation

$$\gamma = \frac{3\pi}{4}\frac{L}{D_l} > 2.35 \ . \tag{22}$$

With $\bar{\eta} = \mathcal{O}\left(\theta^{\geq 4}\right)$, the last term of Eq. (21) represents a perturbation of the Schwarzschild lensing. We look for solutions therefore in the form

$$\widetilde{\theta} = \theta_{1,2}\left[1 + \mathcal{T}(\beta, \gamma, s, \bar{\varepsilon}, \bar{\eta})\right] \ ,$$

with $\mathcal{T}\theta_{1,2}$ a correction to the Schwarzschild images located at $\theta_{1,2}$. The solutions are

$$\mathcal{T}_{1,2} = \frac{s\gamma\left(\bar{\eta} - 5\bar{\varepsilon}^2\right)}{\theta_{1,2}\left(-3\theta_{1,2}^2 + 2\beta\theta_{1,2} + 4\bar{\varepsilon}\right)} \ . \tag{23}$$

We have employed that at $\theta_{1,2}$ the sign $s = \pm 1$. There are two images, located at

$$\widetilde{\theta}_{1,2} \ = \theta_{1,2} \mp \mathcal{A}_{1,2} \tag{24}$$

$$\mathcal{A}_{1,2} \equiv \ - s\theta_{1,2}\mathcal{T}_{1,2} = \frac{\gamma\left(\bar{\eta} - 5\bar{\varepsilon}^2\right)}{\beta\theta_{1,2} + 8\bar{\varepsilon}} \ . \tag{25}$$

The second form of the expressions $\mathcal{A}_{1,2}$ eliminates the quadratic term in $\theta_{1,2}$ appearing in Eq. (23) by using Eq. (15). By employing in the first form of $\mathcal{A}_{1,2}$ the explicit expressions for $\theta_{1,2}$, and introducing the variables $x^{\pm} = \widetilde{\theta}_{1,2}/\theta_E$, $x_0^{\pm} = \theta_{1,2}/\theta_E$, $y = \beta/\theta_E$, also the notation $d_{RN} = \gamma\left(5\bar{\varepsilon} - \bar{\eta}/\bar{\varepsilon}\right)/4\theta_E$ we recover§ Eq. (21) of Ref. [36], derived for Reissner-Nordström black holes. Our result however also covers the negative tidal charge case, which has no analogue in general relativity.

At perfect alignment $\beta = 0$, the second order accuracy Einstein ring appears, as

$$\widetilde{\theta}_E = \theta_E - \frac{\gamma}{8}\left(\frac{\bar{\eta}}{\bar{\varepsilon}} - 5\bar{\varepsilon}\right) \ . \tag{26}$$

The second order correction to the Schwarzschild images and Einstein ring computed here are of relative order $\mathcal{O}(\theta)$, compared to the respective first order expressions, as expected.

4.1. Magnification factors

In this subsection we compute the corrections to the Schwarzschild magnification (18). For this we employ the second expression (24) in Eq. (17) and obtain

$$\widetilde{\mu}_{1,2} = \mu_{1,2}\left(1 \mp \frac{\mathcal{A}_{1,2}}{\theta_{1,2}}\frac{8\bar{\varepsilon} \pm \beta\mathcal{A}_{1,2}}{8\bar{\varepsilon} + \beta\theta_{1,2}}\right) \pm \frac{\theta_{1,2}}{\beta}\frac{\mathcal{A}_{1,2}\left(\theta_{1,2} \mp \mathcal{A}_{1,2}\right)}{\beta\theta_{1,2} + 8\bar{\varepsilon}} \ . \tag{27}$$

For $\mathcal{O}(\beta) \approx \mathcal{O}(\theta)$ to leading order in θ and employing $\bar{\varepsilon} = \theta_E^2/4$ we are left with

$$\widetilde{\mu}_{1,2} = \mu_{1,2}\left(1 \mp \frac{2\theta_E^2\mathcal{A}_{1,2}}{\left(2\theta_E^2 + \beta\theta_{1,2}\right)\theta_{1,2}}\right) \pm \frac{\mathcal{A}_{1,2}\theta_{1,2}^2}{\beta\left(2\theta_E^2 + \beta\theta_{1,2}\right)} \ . \tag{28}$$

We show in Fig 3 the image separations, the magnifications of the two images and their ratio for both the perturbed and Schwarzschild cases for the case where $\gamma\left(\bar{\eta} - 5\bar{\varepsilon}^2\right) = 10^{-1}\theta_E^3$. This figure is an analogue of Fig. 2.4. of Ref. [41].

The image separation slightly decreases in the perturbed case, with a difference independent of β between the tidal charged and the Schwarzschild black holes. The primary image magnification is negligibly affected, while the changes in the magnification of the secondary image are more significant and lead to a lessening of its brightness. This effect can be expected from the fact that the bending angle for the secondary image is greater than that for the primary, and therefore creates a greater sensitivity to changes in the the geometry. Finally, the differences in the magnification ratios $(\tilde{\mu}_1/\tilde{\mu}_2)$ for the two black holes are most apparent as β increases: the magnification ratio is significantly larger in the perturbed case. From an observational point of view such a measure should provide the best means to distinguish between the two black hole geometries.

§ Without the index 1 on the left hand side of the respective equation, which is a typo.

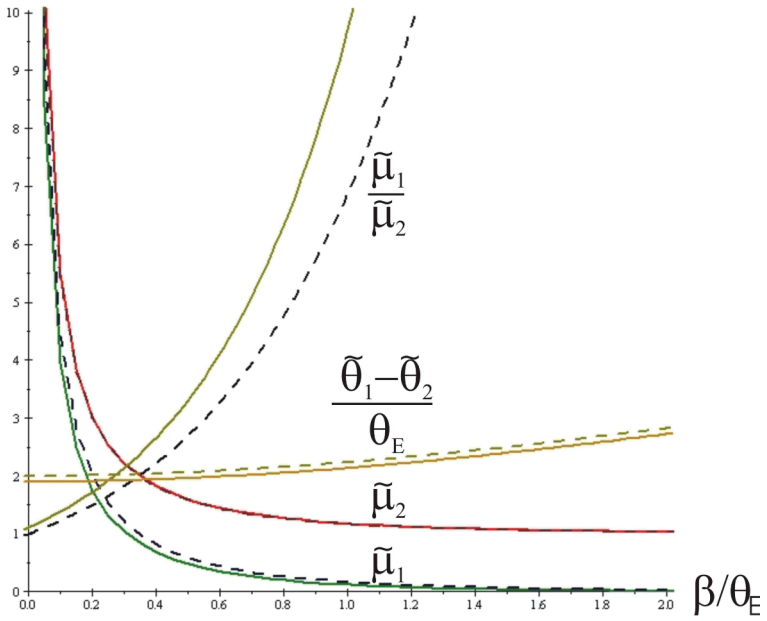

Figure 3. (Colour online.) The image separations, the magnifications of the two images and their ratio as functions of β/θ_E for the perturbed case (solid lines) as compared to the Schwarzschild case (dashed lines) for the parameter values $\gamma\left(\bar{\eta}-5\bar{\varepsilon}^2\right)=10^{-1}\theta_E^3$. From top to bottom at $\beta/\theta_E=0.8$ they are the flux ratio $\widetilde{\mu}_1/\widetilde{\mu}_2$, the image separation $(\widetilde{\theta}_1-\widetilde{\theta}_2)/\theta_E$, the magnification of the primary image $\widetilde{\mu}_1$ and finally the magnification of the secondary image $\widetilde{\mu}_2$. The largest effect can be seen on the flux ratios.

We have checked that in the situation where $\bar{\eta}-5\bar{\varepsilon}^2<0$, the changes with respect to the Schwarzschild black hole lensing will be reversed. The image separation and the secondary image magnification increase, while the magnification ratio decreases.

5. Tidal charge dominated weak lensing to first order

Under the assumptions B) of Section 3 the lens equation (12) reduces to

$$0=\cos^2\theta\ \left(\tan|\theta|-s\tan\beta\right)+\bar{\eta}\frac{3\pi}{4}\frac{L}{D_l}\cot|\theta|\left(\cot|\theta|+s\frac{L}{D_l}\tan\beta\right)\ . \quad (29)$$

The expansion in θ and β to leading order yields (assuming $\bar{\eta}=\mathcal{O}\left(\theta^3\right)$, which turns out to be the weak lensing condition for the tidal charge dominated black hole):

$$0=\theta^3-\beta\theta^2+s\gamma\bar{\eta}\ . \quad (30)$$

Here again, without tidal charge there is no deflection ($\beta=\theta$).

The tidal charge causes a small deflection, which will be discussed in what follows. In the process we need to identify real roots of the third rank polynomial and give them in manifestly real form. We proceed as follows. The discriminant of the third rank polynomial on the right hand side of Eq. (30) is

$$\Delta=s\bar{\eta}\gamma\left(-\frac{\beta^3}{27}+\frac{s\bar{\eta}\gamma}{4}\right)\ . \quad (31)$$

There is one real root when $\Delta > 0$. This situation occurs when either $s\bar{\eta} < 0$ or $s\bar{\eta} > 4\beta^3/27\gamma$. Otherwise, when $0 < s\bar{\eta} \leq 4\beta^3/27\gamma$ there are three real roots (two of them being equal, when the equality holds). The case $s\bar{\eta} = 0$ would mean no deflection, thus it is excluded (we assume non-collinearity, $\beta \neq 0$). We discuss the individual cases as follows:

Case $s\bar{\eta} < 0$. The polynomial (30) has one real root $\theta_{\eta 1}$, which is an image only if it obeys sgn $\theta_{\eta 1} \equiv s = -$sgn $\bar{\eta}$. The real root (obtained by the Cardano formula)

$$\theta_{\eta 1} = \frac{\beta}{3} + \frac{2\beta}{3}\cosh\omega_1 > \beta \ , \tag{32}$$

is positive, thus $s = 1$. Here we have introduced the notation

$$\omega_s = \frac{1}{3}\text{arc}\cosh\left(s - \frac{27}{2}\frac{\gamma\bar{\eta}}{\beta^3}\right) \ . \tag{33}$$

This image arises due to a negative tidal charge, which has the same type of lensing effect as the mass would have in the Schwarzschild case (Fig 1.a).

We will identify the second image $\theta_{\eta 2}$, which forms below the optical axis, by analyzing the remaining two cases. Both these cases obey $s\bar{\eta} > 0$, thus sgn $\theta_{\eta 2} = s =$sgn $\bar{\eta}$. They include images formed below the optical axes ($s = -1$) only for negative tidal charges (Fig 1.b); and above the optical axis ($s = 1$) only for positive tidal charges (which generate a repulsive, scattering effect, see Fig 1.c). As there are two sign changes in the polynomial (30), from the generic theory of polynomials we expect an even number of positive roots. We discuss these two cases in what follows.

Case $s\bar{\eta} > 4\beta^3/27\gamma$. The polynomial (30) has one real root $\theta_{\eta 2}$. The Cardano formula gives a negative root,

$$\theta_{\eta 2} = \frac{\beta}{3} - \frac{2\beta}{3}\cosh\omega_{-1} \leq -\frac{\beta}{3} \ , \tag{34}$$

therefore $s = -1$ holds. This is the second image due to a negative tidal charge.

Case $0 < s\bar{\eta} \leq 4\beta^3/27\gamma$. The polynomial (30) has three real roots, one negative

$$\theta'_{\eta 2} = \frac{\beta}{3} + \frac{2\beta}{3}\cos\varphi_{-1} \in \frac{\beta}{3}[-1, 0) \ , \tag{35}$$

($\cos\varphi_{-1} \in [-1, -1/2)$) and two positive

$$\theta''_{\eta 2} = \frac{\beta}{3} + \frac{2\beta}{3}\cos\left(\varphi_1 + \frac{2\pi}{3}\right) \in (0, \beta) \ . \tag{36}$$

$$\theta''_{\eta 1} = \frac{\beta}{3} + \frac{2\beta}{3}\cos\left(\varphi_1 - \frac{2\pi}{3}\right) \in (0, \beta) \ . \tag{37}$$

Here we have introduced the notation

$$\varphi_s = \frac{1}{3}\arccos\left(1 - \frac{27}{2}s\frac{\gamma\bar{\eta}}{\beta^3}\right) + \frac{2\pi}{3}. \tag{38}$$

We remark, that $\theta''_{\eta 2} < \theta''_{\eta 1}$ on the whole range, with the exception of $\bar{\eta} = 4\beta^3/27\gamma$, where $\theta''_{\eta 1} = \theta''_{\eta 2} = 2\beta/3$.

The negative root $\theta'_{\eta 2}$ corresponds to a negative tidal charge, which is the second image corresponding to $\theta_{\eta 1}$ in the range of parameters covered in this case. The positive

roots $\theta''_{\eta 1}$, $\theta''_{\eta 2}$ correspond to a positive tidal charge, which induces a scattering (a lensing with $\delta < 0$).

In the $\bar{\eta} \to 0$ limit, we expect the image at β. Indeed, $\omega_s = 0$, $\varphi = 2\pi/3$, thus $\theta_{\eta 1} \to \beta$ and $\theta'_{\eta 2} \to 0$ for $\bar{\eta} < 0$ (this being in perfect analogy with the behaviour of the Schwarzschild images $\theta_{1,2}$ in the $\bar{\varepsilon} \to 0$ limit); while $\theta''_{\eta 2} \to 0$ and $\theta''_{\eta 1} \to \beta$ for $\bar{\eta} > 0$.

5.1. Summary of the image positions

For negative tidal charge we obtained two images, $\theta_{\eta 1}$ appearing above the optical axis, and (depending on the magnitude of the tidal charge) either $\theta_{\eta 2}$ or $\theta'_{\eta 2}$, appearing below the optical axis. We remark here, that by the identity $\cosh x = \cos ix$ one can show that $\varphi = \pi - i\omega_{-1}$ holds, such that the two expressions can be shown to be identical, $\theta'_{\eta 2} \equiv \theta_{\eta 2}$. However only one of the expressions $\theta'_{\eta 2}$ and $\theta_{\eta 2}$ is manifestly real, each in its domain of validity.

For positive tidal charge we have obtained two images $\theta''_{\eta 1}$, $\theta''_{\eta 2}$ of the type represented on Fig 1(b). The possibility to have more then one such trajectory for a given configuration of the source, lensing object and observer is encoded in the fact that the deflection is stronger as we approach the black hole. This is in perfect analogy with the scattering produced by a negative mass Schwarzschild centre (a naked singularity), discussed in Ref. [38]. Another similarity is the existence of an upper limit $\bar{\eta}_{\max} = 4\beta^3/27\gamma$, which is the largest value capable of producing scattered images.

The image locations for the different ranges of $\bar{\eta}$ are presented in Fig 4.

5.2. Einstein rings formed by tidal charged lenses without mass

When $\beta = 0$, Eq. (30) becomes

$$0 = \ |\theta|^3 + \bar{\eta}\gamma \ . \tag{39}$$

This has no solution for positive tidal charge. For negative tidal charge we get the analogue of the Einstein ring at $\theta_{\eta E} = \gamma^{1/3} \left|\bar{\eta}\right|^{1/3}$.

Due to the presence of β in the denominators, the $\beta \to 0$ limit cannot be obtained directly from the analytical expressions for $\theta_{\eta 1}$, $\theta_{\eta 2}$ and $\theta'_{\eta 2}$. We have checked, using the l'Hospital rule that $\lim_{\beta\to 0} \theta_{\eta 1} = -\lim_{\beta\to 0} \theta_{\eta 2} = -\lim_{\beta\to 0} \theta'_{\eta 2} = \theta_{\eta E}$.

5.3. Magnification factors

The magnification factor for each of the images discussed above, namely; $\theta_{\eta 1,2}$, $\theta'_{\eta 2}$ and $\theta''_{\eta 1,2}$, respectively are found to be

$$\mu_{\eta 1,2} = \frac{2}{9}\sqrt{\frac{27\theta_{\eta E}^3}{27\theta_{\eta E}^3 \mp 4\beta^3}}\left(2\cosh\omega_{\pm 1} \pm 1\right)\sinh\omega_{\pm 1} + \frac{\left(1 \pm 2\cosh\omega_{\pm 1}\right)^2}{9} \tag{40}$$

$$\mu'_{\eta 2} \ = \frac{-2}{9}\sqrt{\frac{-27\theta_{\eta E}^3}{27\theta_{\eta E}^3 + 4\beta^3}}\left(2\cos\varphi_{-1} + 1\right)\sin\varphi_{-1} + \frac{\left(1 + 2\cos\varphi_{-1}\right)^2}{9} \ , \tag{41}$$

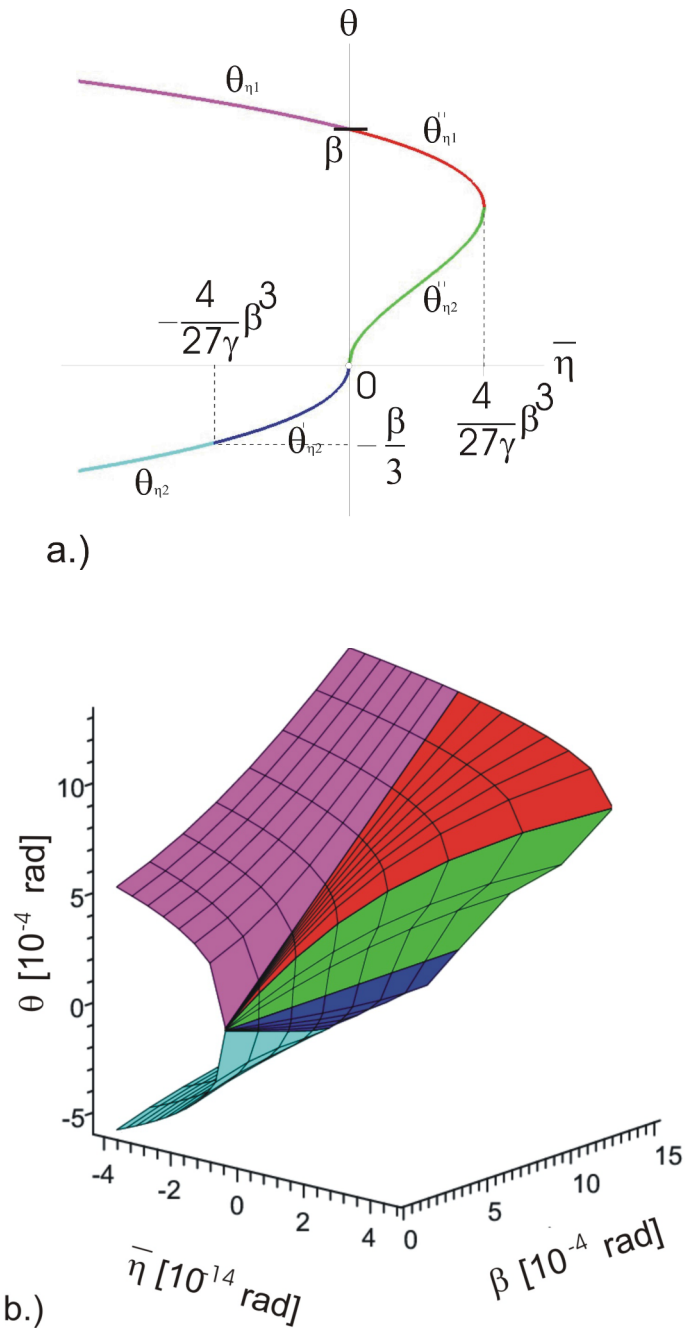

Figure 4. (Colour online.) When the tidal charge dominates over the mass in the lensing, there are still two images, but different from the Schwarzschild case. (a) The position θ (in units of β) of the images for tidal charge dominated black holes characterized by the parameter $\bar{\eta}$. For negative tidal charge ($\bar{\eta} < 0$) there are two images, situated above and below the optical axis. For positive tidal charge ($\bar{\eta} > 0$) both images lie above the optical axis. The images coincide for $\bar{\eta} = 4\beta^3/27\gamma$. For each β, the positive tidal charges with $\bar{\eta} > 4\beta^3/27\gamma$ do not allow for any image. The colours distinguish the images obtained as distinct analytic expressions, which however generate a globally continuous curve. (b) θ as function of $\bar{\eta}$ and β. With decreasing β, the images shrink accordingly. At $\beta = 0$, the angle θ represents the angular radius of the Einstein ring (therefore the $\beta = 0$ section of the surface is symmetric with respect to $\theta = 0$).

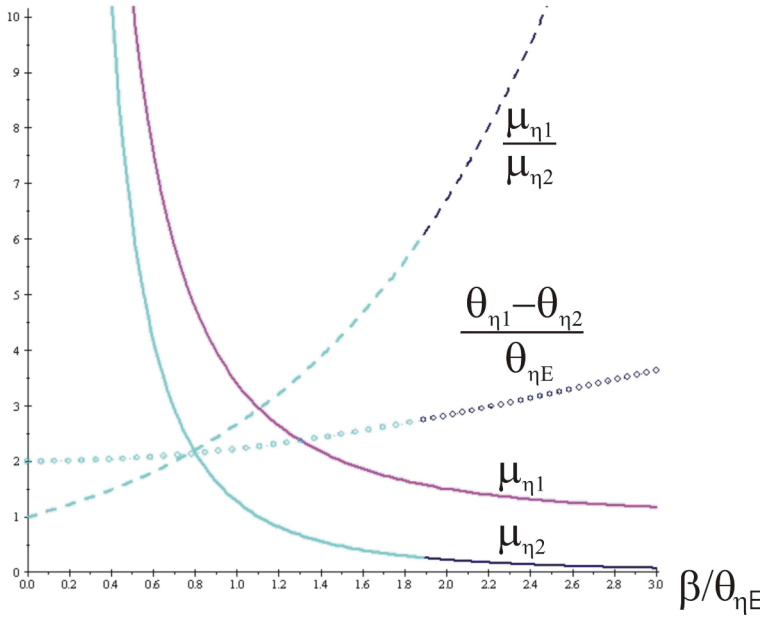

Figure 5. (Color online.) Image separations and magnifications for a negative tidal charge dominated black hole, as functions of $\beta/\theta_{\eta E}$. The upper and lower solid curves plot the primary and secondary image magnification factors, respectively; their ratio is the dashed curve; and the dotted curve is the image separation. A color change at $3/4^{1/3}$ represents the change in functional form from $\theta_{\eta 2}$ (left) to $\theta'_{\eta 2}$ (right).The colours match those of Fig 4.

$$\mu''_{\eta 1,2} = \pm \frac{2}{9}\sqrt{\frac{27\theta_{\eta E}^3}{-27\theta_{\eta E}^3+4\beta^3}}\left[2\cos\left(\varphi_1 \mp \frac{2\pi}{3}\right)+1\right]\sin\left(\varphi_1 \mp \frac{2\pi}{3}\right) \pm \frac{1}{9}\left[1+2\cos\left(\varphi_1 \mp \frac{2\pi}{3}\right)\right]^2 , \tag{42}$$

In Fig 5 we have represented the normalized image separations in units of $\theta_{\eta E}$, the magnification factors and the flux ratios for a negative tidal charge as function of $\beta/\theta_{\eta E}$. The image $\theta_{\eta 2}$ arises for $\bar{\eta} \leq -4\beta^3/27\gamma$ (thus $-\theta_{\eta E} \leq -4^{1/3}\beta/3$), such that $\beta/\theta_{\eta E} \leq 3/4^{1/3} = 1.8899$ while the image $\theta'_{\eta 2}$ for $-4\beta^3/27\gamma \leq \bar{\eta} \leq 0$ (thus $-4^{1/3}\beta/3 \leq -\theta_{\eta E} \leq 0$), such that $\beta/\theta_{\eta E} \geq 3/4^{1/3}$. By contrast, the image $\theta_{\eta 1}$ arises for any $\bar{\eta} \leq 0$. Therefore we have plotted $(\theta_{\eta 1} - \theta_{\eta 2})/\theta_{\eta E}$, $\mu_{\eta 1}$, $\mu_{\eta 2}$, and $\mu_{\eta 1}/\mu_{\eta 2}$ in the range $\beta/\theta_{\eta E} \in \left[0, 3/4^{1/3}\right]$ while $\left(\theta_{\eta 1} - \theta'_{\eta 2}\right)/\theta_{\eta E}$, $\mu_{\eta 1}$, $\mu'_{\eta 2}$, and $\mu_{\eta 1}/\mu'_{\eta 2}$ in the range $\beta/\theta_{\eta E} \geq 3/4^{1/3}$.

As for Schwarzschild case, the image separation and the flux ratio are monotonically increasing functions of the source angle β, while the magnification factors decrease with increasing β, and diverge for $\beta \to 0$. Also the flux ratio goes to unity as $\beta \to 0$. The most obvious difference between the tidal charge dominated spacetime and the Schwarzschild case is that for a fixed value of the image separation, the magnification factors are significantly increased in the former. Unfortunately a measurement of the individual magnification factors requires a knowledge of the unlensed source brightness.

However if the images can be resolved to obtain their angular separation and individual brightnesses one can compare the ratio of the magnification factors as a function of the image separation normalized to the Einstein angle for the system. This has the advantage of not having to refer to the unlensed source brightness and normalizes the image separation using the characteristic lensing parameters.

Figure 6 plots the logarithm of the ratio of the primary magnification to the secondary magnification as a function of the logarithm of the image separation divided by the Einstein angle. For image separations greater than about 2.5 times the Einstein angle, the ratio of the magnification factors for each image obeys a power law relationship. Since this leads to an independence of scaling, we suggest that observations of image brightnesses and image separations should be able to distinguish easily between the standard Schwarzschild spacetime and that governed by higher-dimensional Weyl curvature effects that induce the tidal charge. Given that the magnification of the secondary image produced by the Schwarzschild lens is significantly reduced, the ratio μ_1/μ_2 is much larger than that for the tidally charged lens. Thus for large image separations one has the relation:

$$\mu_1/\mu_2 \approx [\Delta\theta/\theta_E]^{\kappa}$$

In the case of Schwarzschild lensing $\kappa = 6.22 \pm .15$ where as for the tidally charged black hole lensing one obtains $\kappa_\eta = 2.85 \pm .25$, which gives two completely different power law behaviours.

Therefore given a large enough number of measurements of image separations and image brightnesses (as well as a knowledge of the characteristics of the lensing object) such a relationship should provide a very good observational signature that might distinguish between the lensing behaviour by the two types of black holes.

In Fig 7 we have represented the image separations $\left(\theta''_{\eta 1} - \theta''_{\eta 2}\right) / \left(\gamma\bar{\eta}\right)^{1/3}$, magnification factors $\mu''_{\eta 1,2}$ and flux ratios $\mu''_{\eta 1}/\mu''_{\eta 2}$ for a positive tidal charge as function of $\beta/\left(\gamma\bar{\eta}\right)^{1/3}$. As the allowed positive tidal charged parameter range is $0 \leq \bar{\eta} \leq 4\beta^3/27\gamma$ (thus $0 \leq \left(\gamma\bar{\eta}\right)^{1/3} \leq 4^{1/3}\beta/3$), the range of the variable $x = \beta/\left(\gamma\bar{\eta}\right)^{1/3}$ is restricted to $x \geq 3/4^{1/3}$. This is very similar to the negative mass Schwarzschild lensing, also shown on Fig 7.

6. Tidal charge dominated weak lensing to second order

In this section we follow the method presented in section 4 for obtaining the second order correction to the tidal charge dominated light deflection. Thus we go to second order in $\bar{\eta}$. The terms $\bar{\varepsilon}^2$ and $\bar{\varepsilon}\bar{\eta}$ can be dropped from the lens equation (12), being considered of higher order. Thus the lens equation (12) reduces to

$$\begin{aligned} 0 = {} & \cos^2\theta\left(\tan\theta - \tan\beta\right) - 4\bar{\varepsilon}\cos\theta\left(\frac{4\gamma}{3\pi}\tan\beta + \cot\theta\right) \\ & + \gamma\bar{\eta}\cot\theta\left(s\cot\theta + \frac{4\gamma}{3\pi}\tan\beta\right) \end{aligned}$$

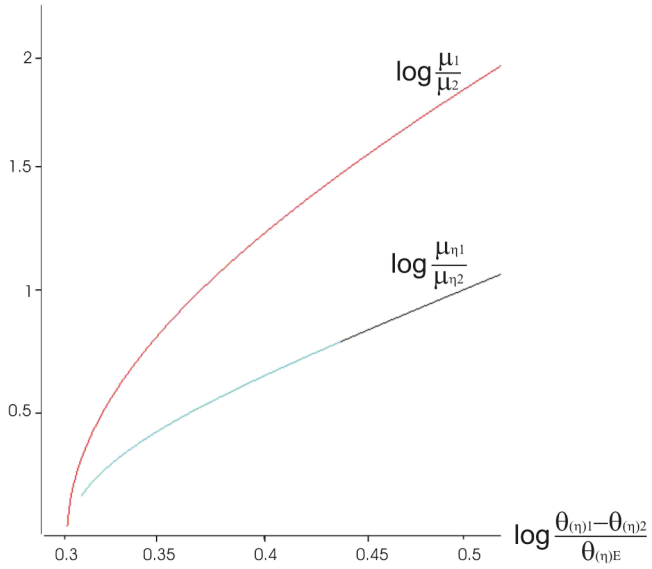

Figure 6. (Color online.) The ratio of the magnification factor of the primary and secondary images as function of the image separation normalized to the Einstein angle, on log-log scale, for the tidal charge dominated black hole and Schwarzschild black hole. The tidal charged case is distinguished by the use of the η-subscript.

$$-\frac{\gamma^3}{9\pi^2}\bar{\eta}^2\frac{\cos\theta}{\sin^3\theta}\left[\frac{4\gamma}{3\pi}\tan\beta\left(6\pi\cot\theta-35s\right)-6\pi-35s\cot\theta\right]\ . \tag{43}$$

By taking $\bar{\eta}=\mathcal{O}\left(\theta^3\right)$ in accordance with the reasoning of section 5, and a higher order mass parameter $\bar{\varepsilon}=\mathcal{O}\left(\theta^{\geq 4}\right)$, the expansion in θ and β yields

$$\begin{aligned} 0\ &=\theta-\beta+\frac{s\gamma\bar{\eta}}{\theta^2}+\mathcal{U}\left(\bar{\varepsilon},\bar{\eta},s,\theta\right)\ , \\ \mathcal{U}\ &=\ -\frac{35s\gamma^3}{9\pi^2}\frac{\bar{\eta}^2}{\theta^4}+\mathcal{U}_3\ , \end{aligned} \tag{44}$$

where $\mathcal{U}_3$ represents third order terms in θ as follows

$$\begin{aligned} \mathcal{U}_3 =\ &-\frac{2\theta+\beta}{3}\left(\theta-\beta\right)^2-\frac{4\bar{\varepsilon}}{\theta} \\ &-\frac{2s\gamma\bar{\eta}}{3}+\frac{4\gamma^2\beta\,\bar{\eta}}{3s\pi\,\theta}-\frac{2\gamma^3\bar{\eta}^2}{3\pi\,\theta^3}\ +\frac{8\,\gamma^4\beta\bar{\eta}^2}{9\pi^2\theta^4}\ . \end{aligned} \tag{45}$$

According to our assumptions the leading order term due to the mass enters here, therefore we need to keep all other terms of this order. Note that some of these terms differ from the respective terms arising from the Virbhadra-Ellis lens equation (10), as can be checked from the Appendix.

We also remark, that without mass and tidal charge there is no deflection at all ($\theta=\beta$ is a solution when $\bar{\varepsilon}=\bar{\eta}=0$), as expected.

The term $\mathcal{U}$ represents a perturbation of the tidal charge dominated weak lensing discussed in the previous section, Eq. (30) and is of $\mathcal{O}\left(\theta^{\geq 2}\right)$. We look for solutions

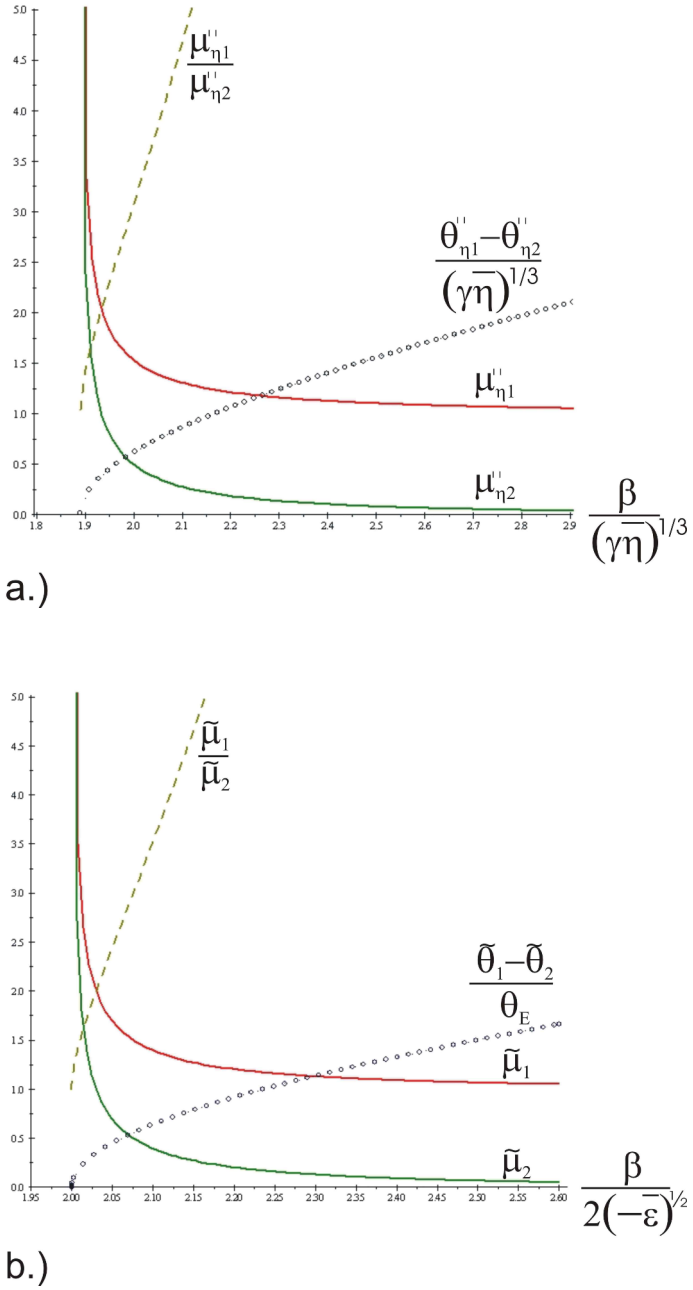

Figure 7. (Color online.) Image separations and magnifications for a positive tidal charge dominated black hole (a), as functions of $\beta/\left(\gamma\bar{\eta}\right)^{1/3}$. The upper and lower solid curves plot the primary and secondary image magnification factors, respectively; their ratio is the dashed curve; and the dotted curve is the image separation. The colours match those of Fig 4. The negative mass Schwarzschild geometry produces similar lensing effects (b), in terms of the independent variable $\beta/2\left(-\bar{\varepsilon}\right)^{1/2}$.

therefore in the form

$$\widetilde{\theta} = \theta\left[1 + \mathcal{T}_\eta\left(\bar{\varepsilon}, \bar{\eta}, s, \beta\right)\right] \ . \tag{46}$$

In what follows we will show that the correction term $\mathcal{T}_\eta$ is $\mathcal{O}\left(\theta\right)$.

6.1. Positive $\bar{\eta}$

We look for the corrections $(\mathcal{T}_\eta)_\pm (\theta_\eta)_\pm$ of the images $(\theta_\eta)_\pm$ located at (32), (34). The solutions are

$$(\mathcal{T}_\eta)_\pm = \frac{(\theta_\eta)_\pm^2 \mathcal{U}\left(\bar{\varepsilon}, \bar{\eta}, s, (\theta_\eta)_\pm\right)}{2\gamma\bar{\eta} - s\,(\theta_\eta)_\pm^3} \ . \tag{47}$$

There are two images, located at $\left(\widetilde{\theta}_\eta\right)_\pm = (\theta_\eta)_\pm \left[1 + (\mathcal{T}_\eta)_\pm\right]$.

6.2. Negative $\bar{\eta}$

We look for the corrections $(\mathcal{T}_\eta)_{1.2} (\theta_\eta)_{1,2}$ of the images $(\theta_\eta)_{1,2}$ located at (32), (34). The solutions are

$$(\mathcal{T}_\eta)_{1.2} = \frac{(\theta_\eta)_{1,2}^2 \mathcal{U}\left(\bar{\varepsilon}, \bar{\eta}, s, (\theta_\eta)_{1,2}\right)}{2\gamma\bar{\eta} - s\,(\theta_\eta)_{1,2}^3} \ . \tag{48}$$

There are two images, located at $\left(\widetilde{\theta}_\eta\right)_{1,2} = (\theta_\eta)_{1,2} \left[1 + (\mathcal{T}_\eta)_{1.2}\right]$.

7. Concluding remarks

Using simple geometric relations we derived a generic lens equation, Eq. (6) for weak lensing. This formula is more accurate than the Virbhadra-Ellis lens equation (as it contains no approximations of trigonometric expressions), but reduces to it in a proper limit (differences are to be expected in asymmetric source and observer distances with respect to the lens).

We have applied our lens equation in the discussion of the weak lensing by tidal charged black holes, to both first and second order accuracy in the black hole parameters, when either the mass or the tidal charge dominates. We have carried on expansions in the small mass and tidal charge parameters, as well as in the angles spanned by the real and apparent positions of the sources with the optical axis. In the Appendix we have investigated the differences between the predictions of the two lens equations. The predictions of our lens equation (6) and of the Virbhadra-Ellis lens equation (10) coincide in most of the cases we consider, with the notable exception of the tidal charge dominated black hole lensing discussed to a higher accuracy in Section 6, where the Virbhadra-Ellis lens equation would not predict (or would predict with different coefficients) some of the higher order terms.

Although Solar System tests lead to the expected result, that light deflection by the Sun is due to its mass, and leaves room but for a minuscule tidal charge [32], [34], it cannot be excluded that tidal charge dominated black holes could exist on the brane, as the tidal charge is an imprint of the Weyl curvature of the higher-dimensional space-time, which remains unspecified for the tidal charged black hole.

In the case of mass dominated weak lensing, we found that the position of the images is similar to the Reissner-Nordström black hole lensing, discussed in Ref. [36]. We have

analyzed, how the image separations, the magnification factors and the flux ratios are modified as compared to the Schwarzschild lensing by the perturbations arising from second order mass and linear tidal charge contributions ($\bar{\varepsilon}^2$ and $\bar{\eta}$, respectively). The most striking modification appears in the ratio of the magnification factors (the flux ratio), shown on Fig 3, which can be either increased or decreased, depending on the sign of $\bar{\eta} - 5\bar{\varepsilon}^2$.

When the tidal charge dominates in the lensing behaviour, the situation is different. The case of positive tidal charge resembles the lensing properties of a negative mass Schwarzschild spacetime [38].

Black holes with negative tidal charge are however favoured by strengthening and confining gravity to the brane and also by thermodynamic considerations [42]. In the case of a dominant negative tidal charge the lensing properties are similar to those of a positive mass Schwarzschild black hole, where the similarity is only in the number of images lying above or below the optical axis. The actual location of the images is different and this fact is summarized in Fig 4, which is one of the main results of this paper.

Finally the power law dependence of the ratio of the magnification factors on the separation of the images provides an means for observing the differences between the Schwarzschild and tidal charged black holes. Given that the next generation of radio telescopes will easily be able to resolve images to less than milli-arcsecond accuracy, the different rates at which the ratio of the brightness changes should be able to provide a significant observational signature to constrain the Weyl curvature as a substitute for dark matter.

Acknowledgements

ZsH and LÁG were supported by the Hungarian Scientific Research Fund (OTKA) grants no. 69036 and 81364, respectively.

Appendix A. Comparing our lens equation with the Virbhadra-Ellis lens equation

In this Appendix we present the explicit form of our lens equation (6) and of the Virbhadra-Ellis lens equation (10), both to fourth order in θ, adopting the minimal assumptions $\bar{\varepsilon} = \mathcal{O}\left(\theta^{\geq 2}\right)$ and $\bar{\eta} = \mathcal{O}\left(\theta^{\geq 3}\right)$, which cover all cases considered in the main text. These particular cases can be recovered by shifting the θ-order of the parameters $\bar{\varepsilon}$ and $\bar{\eta}$, as described at the beginning of each section, and dropping the terms, which fall beyond the desired accuracy.

The lens equation (6) in detail reads:

$$0 = L_0^{HGH} + \bar{\varepsilon} L_{10}^{HGH} + \bar{\eta} L_{01}^{HGH} + \bar{\varepsilon}^2 L_{20}^{HGE} + \bar{\varepsilon}\bar{\eta} L_{11}^{HGH} + \bar{\eta}^2 L_{02}^{HGH} \ , \qquad \text{(A.1)}$$

with the coefficients

$$
\begin{aligned}
L_0^{HGH} &= (\theta-\beta)\left[1-\frac{(2\theta+\beta)(\theta-\beta)}{3}\right] ,\\
L_{10}^{HGH} &= -\frac{4}{\theta}+\frac{2}{3}\left(5\,\theta\ -\frac{8\gamma\beta}{\pi}\right) ,\\
L_{01}^{HGH} &= \frac{s\,\gamma}{\theta^2}-\frac{2s\gamma}{3}\left(1-\frac{2\gamma\beta}{\pi\,\theta}\right) ,\\
L_{20}^{HGE} &= -\frac{5s\gamma}{\theta^2}-\frac{32\gamma}{3\pi\,\theta}\left(1\ -\frac{4\gamma\beta}{3\pi\theta}\right)+\frac{10s\gamma}{3}\left(1-\frac{2\gamma\beta}{\pi\,\theta}\right) ,\\
L_{11}^{HGH} &= \frac{256\gamma^2}{9\pi^2\theta^3}+\frac{16s\gamma^2}{3\pi\,\theta^2}\left(1-\frac{4\gamma\beta}{3\pi\theta}\right)-\frac{128\gamma^2}{9\pi^2\theta}\left(1-\frac{8\gamma\beta}{3\pi\theta}\right) ,\\
L_{02}^{HGH} &= -\frac{35s\gamma^3}{9\pi^2\theta^4}-\frac{2\gamma^3}{3\pi\,\theta^3}\left(1-\frac{4\gamma\beta}{3\pi\theta}\right)+\frac{35s\gamma^3}{27\pi^2\theta^2}\left(1-\frac{4\gamma\beta}{\pi\theta}\right) .
\end{aligned}
\tag{A.2}
$$

The Virbhadra-Ellis lens equation (10) gives:

$$
0 = L_0^{VE}+\bar{\varepsilon}L_{10}^{VE}+\bar{\eta}L_{01}^{VE}+\bar{\varepsilon}^2L_{20}^{VE}+\bar{\varepsilon}\bar{\eta}L_{11}^{VE}+\bar{\eta}^2L_{02}^{VE} . \tag{A.3}
$$

The coefficients in (A.3) are:

$$
\begin{aligned}
L_0^{VE} &= (\theta\ -\beta)\left(1+\frac{\theta^2+\beta^2+\theta\beta}{3}\right) ,\\
L_{10}^{VE} &= -\frac{4}{\theta}-\frac{14\theta}{3} ,\\
L_{01}^{VE} &= \frac{s\,\gamma}{\theta^2}+\frac{4s\gamma}{3} ,\\
L_{20}^{VE} &= -\frac{5s\gamma}{\theta^2}+\frac{64\gamma}{3\pi\theta}-\frac{20s\gamma}{3} ,\\
L_{11}^{VE} &= \frac{256\gamma^2}{9\pi^2\theta^3}-\frac{32s\gamma^2}{3\pi\,\theta^2}+\frac{128\gamma^2}{3\pi^2\theta} ,\\
L_{02}^{VE} &= -\frac{35s\gamma^3}{9\pi^2\theta^4}+\frac{4\gamma^3}{3\pi\,\theta^3}-\frac{175s\gamma^3}{27\pi^2\theta^2} .
\end{aligned}
\tag{A.4}
$$

One can see, that all coefficients are different in the two approaches by terms, which in the lens equations are of order $\mathcal{O}\left(\theta^{\geq 3}\right)$. We conclude, that the two lens equations agree only at θ^2 order.

References

[1] P Binétruy, C Deffayet, U Ellwanger and D Langlois 2000 *Phys. Lett.* B **477** 285
[2] P Bostock, R Gregory, I Navarro and J Santiago 2004 *Phys. Rev. Lett.* **92** 221601
[3] C de Rham and A J Tolley 2006 *JCAP* **0602** 003
[4] R Maartens, 2004 *Living Rev. Rel.* **7** 1
[5] T Shiromizu, K Maeda and M Sasaki, 2000 *Phys. Rev.* D **62** 024012
[6] L Á Gergely, 2003 *Phys. Rev.* D **68** 124011
[7] L Á Gergely 2008 *Phys. Rev.* D **78** 084006
[8] M K Mak and T Harko 2004 *Phys. Rev. D* **70** 024010
[9] S Pal, S Bharadwaj and S Kar 2005 *Phys. Lett. B* **609** 194

[10] S Pal 2005 *Phys. Teacher* **47** 144
[11] N Kaloper and D Kiley 2006 *JHEP* **0603** 077
[12] P Kanti and K Tamvakis 2002 *Phys. Rev. D* **65** 084010
[13] P Kanti, I Olasagasti and K Tamvakis 2003 *Phys. Rev. D* **68** 124001
[14] R Emparan, A Fabbri and N Kaloper 2002 *JHEP* **0208** 043
[15] H Kudoh, T Tanaka and T Nakamura 2003 *Phys. Rev. D* **68** 024035
[16] A Chamblin, S W Hawking and H S Reall 2000 *Phys. Rev.* D **61** 065007
[17] R Gregory and R Laflamme 1993 *Phys. Rev. Lett.* **70** 2837
[18] R. Gregory, *Class. Quantum Grav.* 2000 **17** L125
[19] G T Horowitz and K Maeda 2001 *Phys. Rev. Lett* **87** 131301
[20] S S Seahra, C Clarkson and R Maartens 2005 *Phys. Rev. Lett* **94** 121302
[21] L Randall and R Sundrum 1999 *Phys. Rev. Lett.* **83** 4690
[22] J Garriga and T Tanaka 2000 *Phys. Rev. Lett.* **84** 2778
[23] S B Giddings, E Katz and L Randall 2000 *JHEP* **03** 023
[24] L Á Gergely 2006 *Phys. Rev. D* **74** 024002
[25] S Kar and M Sinha, 2003 *Gen. Rel. Grav.* **35** 10
[26] A S Majumdar and N Mukherjee, 2005 *Mod. Phys. Lett.* **A20** 2487
[27] R Whisker, 2005 *Phys. Rev. D* **71** 064004
[28] A S Majumdar and N Mukherjee, 2005 *Int. J. Mod. Phys D* **14** 1095
[29] N Dadhich, R Maartens, P Papadopoulos and V Rezania, 2000 *Phys. Lett.* B **487** 1
[30] K S Virbhadra and G F R Ellis, 2000 *Phys. Rev.* D **62** 084003
[31] K S Virbhadra, 2009 *Phys. Rev.* D **79** 083004
[32] L Á Gergely, Z Keresztes and M Dwornik, 2009 *Class. Quantum Grav.* **26**, 145002
[33] L Á Gergely and B Darázs, 2006 *Publ. Astron. Dep. Eötvös Univ.* **17** 213-219
[34] G C Böhmer, T Harko and F S N Lobo, 2008 *Class. Quantum Grav.* **25** 045015
[35] V Bozza, 2008 *Phys. Rev.* D **78** 103005
[36] M Sereno, 2004 *Phys. Rev.* D **69** 023002
[37] S Frittelli and E T Newman, 1999 *Phys. Rev.* D **59** 124001
[38] J G Cramer, R L Forward, M S Morris, M Visser, G Benford and G A Landis, 1995 *Phys. Rev.* D **51** 3117-3120
[39] P Schneider, 1984 *Astr. Ap.* **140** 119
[40] R Brandford and R Narayan, 1986 *Astroph. J.* **310** 568
[41] P Schneider, J Ehlers and E E Falco, 1992 *Gravitational Lenses*, Springer Verlag New York
[42] L Á Gergely, N Pidokrajt and S Winitzki, 2008 e-print: arXiv:0811.1548